# Characterization of spark-generated *N*-waves in air using an optical schlieren method

Maria M. Karzova,[a),b)] Petr V. Yuldashev,[a)] and Vera A. Khokhlova[c)]
*Faculty of Physics, Moscow State University, Leninskie Gory, Moscow 119991, Russia*

Sébastien Ollivier, Edouard Salze, and Philippe Blanc-Benon
*Laboratoire de Mécanique des Fluides et d'Acoustique, Unité Mixte de Recherche 5509, Centre National de la Recherche Scientifique, Ecole Centrale de Lyon, Université Lyon I, 36 Avenue Guy de Collongue, F-69134 Ecully Cedex, France*

(Received 2 July 2014; revised 7 March 2015; accepted 19 April 2015)

Accurate measurement of high-amplitude, broadband shock pulses in air is an important part of laboratory-scale experiments in atmospheric acoustics. Although various methods have been developed, specific drawbacks still exist and need to be addressed. Here, a schlieren optical method was used to reconstruct the pressure signatures of nonlinear spherically diverging short acoustic pulses generated using an electric spark source (2.5 kPa, 33 $\mu$s at 10 cm from the source) in homogeneous air. A high-speed camera was used to capture light rays deflected by refractive index inhomogeneities, caused by the acoustic wave. Pressure waveforms were reconstructed from the light intensity patterns in the recorded images using an Abel-type inversion method. Absolute pressure levels were determined by analyzing at different propagation distances the duration of the compression phase of pulses, which changed due to nonlinear propagation effects. Numerical modeling base on the generalized Burgers equation was used to evaluate the smearing of the waveform caused by finite exposure time of the high-speed camera and corresponding limitations in resolution of the schlieren technique. The proposed method allows the study of the evolution of spark-generated shock waves in air starting from the very short distances from the spark, 30 mm, up to 600 mm.  [http://dx.doi.org/10.1121/1.4921026]

[OU] Pages: 3244–3252

## I. INTRODUCTION

High-amplitude (>1 kPa) and short duration (tens of microseconds) acoustic pulses are widely used in down-scaled laboratory experiments to simulate sonic boom propagation through atmospheric inhomogeneities,[1–7] problems of architectural acoustics,[8] urban acoustics,[9] and outdoor sound propagation.[10] The most common ways to generate such pulses in air are to use various spark sources: electrical sparks,[11–13] focused laser beams,[14] or explosive-type materials.[15] Spark-generated pulses are commonly called "*N*-waves" because of their shape.[16] However, the actual waveform of such pulses, particularly their rarefaction phase, can be very different from the symmetric shape of an *N*-wave. In the case of shock waves produced by instantaneous energy release, the peak negative pressure is much lower than peak positive pressure and the duration of rarefaction phase is longer than the duration of compression phase.[17,18] Nevertheless, the *N*-wave model is widespread to describe pressure signatures of shock pulses during their propagation in air.[11,12,19] Even if the waveform is not restricted to have the *N*-wave shape in simulations of pulse propagation through homogeneous[12] and turbulent media,[20] the *N*-wave assumption is still often used to set a boundary condition to the model. This simplified assumption may introduce errors, for example, in the simulation of pulse propagation through a caustic, in which the resulting waveform resembles the derivative of an initial wave.[1,20] Accurate measurement of high-amplitude and short-duration acoustic waveforms at distances close to the source is therefore critical to accurately determine the boundary condition for the modeling.

Propagation of spark-generated acoustic pulses in homogeneous air has been studied experimentally by several teams, particularly by Wright and co-workers[11,21,22] and Yuldashev and co-workers.[12,19] Although several methods have been proposed to characterize acoustic fields produced by sparks, certain measurement limitations still exist.

The most common approach is to measure pressure signatures using acoustic microphones. However, the bandwidth of commercially available high-frequency condenser microphones does not typically exceed 150 kHz at −3 dB level, while the spectrum of shock pulses extends up to 1 MHz; in addition, calibration of microphones at high frequencies is often not accurate. A microphone response and the resulting waveform distortions are also dependent on the microphone mounting. This results in significant distortions of the measured waveforms and steep shock fronts.[12,19] In most cases there is no possibility to theoretically estimate these distortions. Moreover, waveform measurements are impossible close to a spark source because maximum

[a)]Also at: Laboratoire de Mécanique des Fluides et d'Acoustique, Unité Mixte de Recherche 5509, Centre National de la Recherche Scientifique, Ecole Centrale de Lyon, Université Lyon I, 36 Avenue Guy de Collongue, F-69134 Ecully Cedex, France.
[b)]Electronic mail: masha@acs366.phys.msu.ru
[c)]Also at: Center for Industrial and Medical Ultrasound, Applied Physics Laboratory, University of Washington, 1013 NE 40th Street, Seattle, WA 98105, USA.

pressure is out of a condenser microphone linear range. In addition, the pressure level is so high that it can damage microphones. Note also that acoustic measurements could be performed using piezoelectric dynamic pressure sensors, which are appropriate in the case of very high amplitude pressure waves (>100 kPa), but their main disadvantage is low sensitivity (14.5 mV/kPa) and resolution (for example, 3.4 Pa for the model 113B28 PCB Piezotronics).

An alternative method to measure shock pulses produced by sparks is to use optical methods instead of microphones. The basic principle of these methods is that the acoustic wave introduces variations of air density and corresponding variations of optical refractive index; as a result, the light beam deflects from its initial direction when passing through an acoustic signal. Among optical techniques, shadowgraphy, schlieren, and interferometry methods can be used to measure shock waves. In a previous work, an optical focused shadowgraphy technique[12] was used to visualize the front shock of spark-generated waves. An estimation of the front shock width and rise time was then obtained, thanks to numerical simulation of optical beam propagation through the shock. A good agreement with the measurements was shown.[12] Although the shadowgraphy technique provided a good temporal resolution of the high amplitude front shock of the pulse, it was not sufficiently sensitive to restore the whole waveform or even the rear shock of the pulse. The reason is that shadowgraphy method is sensitive to the second derivative of pressure, i.e., it captures sharp changes of pressure at the front shock, while smooth variations of pressure in the pulse are missed. Holographic interferometry has been used to visualize explosion-type waves, but the resolution and the accuracy of the restored waveforms were significantly lower than in the microphone measurements.[23] Laser interferometry can also be used to measure high-amplitude and short duration acoustic pulses in air, however, to our knowledge, no quantitative analysis has been performed to this day for shock waves.[24]

Optical schlieren methods are commonly used to analyze acoustic field structure qualitatively.[25,26] The goal of this paper is to demonstrate that the schlieren method is capable to reconstruct absolute pressure signatures of spark-generated acoustic pulses in homogenous air. A high-speed camera was used to capture light rays deflected by refractive index inhomogeneities caused by an acoustic wave. The reconstruction algorithm was based on the fact that the distribution of light intensity in the measured schlieren images is associated with the acoustic wave by the Abel-type transform. This transform contains an unknown normalization constant which does not permit us to determine absolute pressure values, only the shape of an acoustic signal can be reconstructed. Absolute pressure levels were obtained by analyzing lengthening of the compression phase of the pulse with distance caused by amplitude-dependent nonlinear propagation effects. To determine the duration of the compression phase, the propagation of spherical diverging *N*-wave was simulated using the generalized Burgers equation and the effect of smearing the waveform during the exposure time of the high-speed camera was evaluated.

Further content of the paper is organized as follows. The experimental system is described first, followed by a procedure of reconstruction of the acoustic pressure waveforms from schlieren images (Sec. II). The measured dimensionless waveforms are analyzed at different distances starting from 30 mm and up to 600 mm from the spark source in Sec. III A. Simulation results for distortion of the measured waveforms caused by a finite exposure time of the camera are presented and discussed in Sec. III B. The elongation of the compression phase duration as a function of propagation distance is then analyzed to obtain absolute pressure values for the measured pulses (Sec. III C). Advantages and limitations of the optical schlieren method combined with the proposed reconstruction procedure and absolute pressure calibration are compared with measurements performed using acoustic microphones and optical focused shadowgraphy technique (Sec. IV).

## II. MATERIALS AND METHODS

### A. Experimental arrangement for optical measurements

A top view of the experimental setup designed for optical measurements of spark-generated acoustic waves in homogeneous air is shown in Fig. 1. A spark source with a 21 mm gap between tungsten electrodes and with an applied voltage of 15 kV produced high amplitude pressure pulses that readily turned to a shock waveform when propagating from the spark (Fig. 1).[6] The repetition rate of the pulses was 1 Hz; the wavefront was assumed to have a spherical geometry. Acoustic pulses introduced variations of air density and, as a result, variations of the optical refractive index which are schematically shown in Fig. 1 by gradients of the gray color. These variations were visualized using the schlieren method. The schlieren system was composed of a quartz tungsten halogen (QTH) continuous white light source mounted in the geometrical focus of a spherical mirror with 1 m radius of curvature, a beam splitter, an optical knife (a razor edge), and a high-speed Phantom V12 CMOS camera. Light beam was transmitted through the beam splitter and through the test zone of the acoustic pulse propagation.

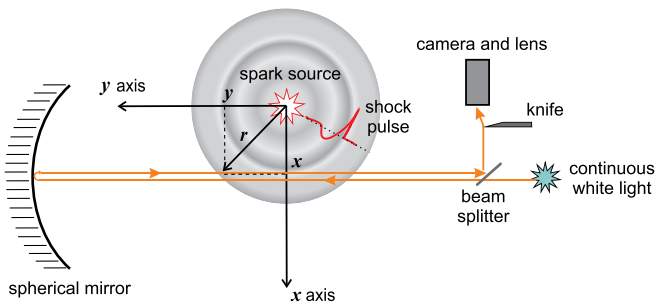


FIG. 1. (Color online) Illustration of the experimental setup, the view is from the top along the $z$ axis. Acoustic pulses are produced by a 15 kV spark source located at $z = 0$. Corresponding variations of the optical refractive index are schematically shown by gradients of the gray color. A schlieren optical system used to visualize the pressure wave consists of QTH continuous light source, a beam splitter, a spherical mirror, an optical knife, and a high-speed camera (Phantom V12 CMOS). Solid lines with arrows illustrate the trajectory of the light beam in the absence of acoustic wave.

Then, the light reflected from the mirror, intersected the test zone once again, and propagated back to the beam splitter (solid lines with arrows in Fig. 1).

Spatial variations of the light refractive index $n$ caused by the acoustic wave led to deviation of a part of light rays from the initial propagation direction. Light rays that were not deflected by acoustic pressure inhomogeneities were blocked by the optical knife located in the focal point of the beam. Deflected rays bent around the razor edge were captured by a high-speed camera to form a schlieren image. Double passing of the light beam through the test zone provided better contrast of the image. The brightness of these images corresponds to modulation of the light intensity and is proportional to the gradient of acoustic pressure.[27]

### B. Theoretical background: Reconstruction of an acoustic waveform from a schlieren image

In this section, the algorithm for reconstructing pressure signatures from schlieren images and corresponding assumptions for its correct interpretation are presented. The proposed method includes two steps. First, the waveforms of acoustic pulses were obtained from schlieren images. Then, the absolute pressure values were determined by analyzing the change in duration of the compression phase of the pulses at different distances from the source.

Acoustic pressure $p$ can be related to the perturbation of the optical refractive index $n$. The refractive index $n$ is related to the air density $\rho_0+\rho$ via the Gladstone–Dale constant $K$ (Ref. 28): $n+n_0=1+K(\rho_0+\rho)$, where $\rho_0$ is the ambient density, and $\rho$ is the density perturbation caused by the acoustic wave, $n_0$ is the ambient refractive index. Under our experimental condition, the density perturbation can be regarded as a linear function of acoustic pressure $p$: $\rho=p/c_0^2$, where $c_0$ is the ambient sound speed; higher order terms can be neglected as the acoustic pressure is small compared to the ambient atmospheric pressure $p_{\text{atm}}$: $p/p_{\text{atm}}\sim 0.01$. The refractive index therefore can be expressed as

$$n=K\frac{p}{c_0^2}. \tag{1}$$

Variation of the refractive index $n$ produces a phase shift $\varphi$ of the light beam. In the $xy$ plane, shown in Fig. 1, the phase shift accumulates while the light propagates along the $y$ axis. Since the phenomenon is symmetrical with respect to the plane $z=0$, the light rays are assumed not to deviate from the $xy$ plane. Neglecting light reflection by acoustic inhomogeneities and taking into account double crossing through the test zone, one can write the phase as $\varphi(x)=2\cdot(2\pi/\lambda)\int_{-\infty}^{+\infty}n(x,y)dy$, where $\lambda$ is the optical wavelength. Radial symmetry of the wavefront allows us to rewrite the expression for the phase as

$$\begin{aligned}\varphi(x)&=2\cdot\frac{2\pi}{\lambda}\int_0^{+\infty}2n\left(r=\sqrt{x^2+y^2}\right)dy\\&=2\cdot\frac{2\pi}{\lambda}\int_x^{+\infty}\frac{2n(r)rdr}{\sqrt{r^2-x^2}}.\end{aligned} \tag{2}$$

Equation (2) is the direct Abel transform of the function $n(r)$.[29] Inversion of the Abel transform (2) and the relationship $s=\lambda\varphi/2\pi$ between the optical path length $s$ and the phase $\varphi$ gives

$$n(r)=-\frac{1}{2\pi}\int_r^{+\infty}\frac{ds}{dx}\frac{dx}{\sqrt{x^2-r^2}}. \tag{3}$$

In the experiments, the light intensity distribution $I$ is the quantity measured in the perpendicular image $xz$ plane of the schlieren arrangement. For a schlieren system, the light intensity of the image formed behind the optical knife is proportional to the angle of deviation of rays.[27] Taking into account the spherical symmetry of the wavefront, the angle of light deviation in the test zone can be written as $\varepsilon=\partial s/\partial r_1$, where $r_1=\sqrt{x^2+z^2}$ is the radial coordinate in the image plane $xz$. Thus, the light intensity $I(r_1)$ in the schlieren image is

$$I(r_1)=-C\frac{\partial s}{\partial r_1}, \tag{4}$$

where $C$ is an unknown constant and the sign minus is introduced to account for the knife orientation. For example, if the knife blocks the light from the opposite side of the beam, the same schlieren image is formed but the bright areas of the image are replaced by the dark ones and vice versa. Integrating the intensity in Eq. (4), one can obtain the optical path length $s$ as

$$s(r_1)=\frac{1}{C}\int_{r_1}^{+\infty}I(r')dr', \tag{5}$$

where $r'$ is a dummy integration variable. Due to the radial symmetry of the optical path length $s$ in the plane $xz$, one could write Eq. (5) in the one dimensional (1D) case of $z=0$,

$$s(x)=\frac{1}{C}\int_x^{+\infty}I(r')dr'. \tag{6}$$

Combining Eqs. (1), (3), and (6) one obtains the following relation between the pressure signature $p$ and the schlieren image intensity $I$:

$$p(r)=-\frac{c_0^2}{2\pi KC}\int_r^{+\infty}\frac{d}{dx}\left(\int_x^{+\infty}I(r')dr'\right)\frac{dx}{\sqrt{x^2-r^2}}. \tag{7}$$

Equation (7) contains the unknown constant $C$, which makes it impossible to reconstruct absolute pressure levels directly from the images. Nonetheless, dimensionless pressure waveforms can be reconstructed by calculating the integral

$$p(r)\sim\int_r^{+\infty}\frac{d}{dx}\left(\int_x^{+\infty}I(r')dr'\right)\frac{dx}{\sqrt{x^2-r^2}}. \tag{8}$$

In order to determine the absolute pressure values in the reconstructed waveforms, the lengthening of the $N$-wave with distance caused by nonlinear propagation effects was

analyzed. The analytic solution of the 1D simple wave equation generalized for spherically divergent waves was used.[30] The duration of the compression phase $T$ at a distance $r$ of a shock wave having an amplitude $p_0$ and a compression phase duration $T_0$ [Fig. 2(a)] at the distance $r_0$ is given by

$$T(r)/T_0 = \sqrt{1 + \sigma_0 \ln(r/r_0)}, \tag{9}$$

where $\sigma_0 = [(\gamma+1)r_0 p_0]/2\gamma p_{atm} c_0 T_0$. Here $\gamma$ is the heat capacity ratio equal to 1.4 for air. In acoustics, Eq. (9) is associated with nonlinear propagation of an ideal spherically divergent $N$-wave, but it also remains valid for nonsymmetrical shock waves if only the compression phase is considered. Equation (9) therefore, can be applied to determine the pressure amplitude $p_0$ from the duration of the compression phase in the waveforms measured at different distances from the spark source. In the schlieren experiment, the spatial extent $d$ of the compression phase of the wave was measured instead of the duration. However, since the acoustic wave does not change greatly over a propagation distance equal to its wavelength, the duration of the compression phase can be related to its spatial extention via the sound speed: $d = Tc_0$.

In our experiment, the duration of the compression phase in the reconstructed dimensionless waveforms was distorted because of a finite exposure time of the high-speed camera, i.e., the shock front was smeared. To simulate the averaging effect induced by the camera, numerical simulations based on the Burgers equation generalized for relaxing homogeneous atmosphere were performed (numerical model is described in detail in the earlier studies in Ref. 12). An ideal spherically diverging $N$-wave was numerically propagated from the source. Then, for each distance where the measurements were taken, the pressure was averaged over all waveforms (100 waveforms total) which passed through this point during the exposure time. The parameters of the initial $N$-wave in the numerical model were: the peak pressure $p_0 = 2500$ Pa at a distance from the spark source $r_0 = 105.6$ mm; the shock rise time, defined as the time during which the acoustic pressure increased from 10% to 90% of the peak positive pressure,[1] was chosen according to the quasi-stationary solution of the Burgers equation as 0.07 $\mu$s; the duration of the compression phase $T_0$ (or the half duration) of the initial $N$-wave, defined as the time between the points of the positive half peak at the front shock and zero

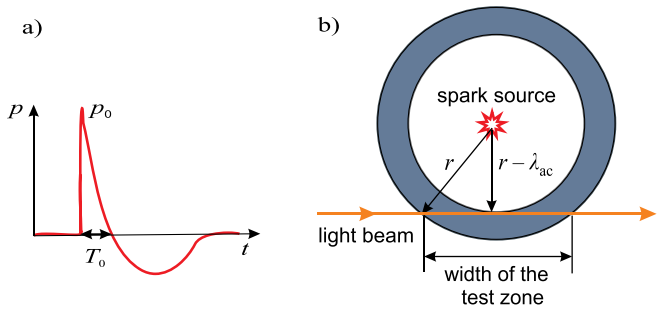


FIG. 2. (Color online) (a) Typical waveform produced by the spark source; $p_0$ and $T_0$ are the peak positive pressure and the duration of the compression phase, correspondingly. (b) Sketch illustrating the calculation of the width of the test zone. Location of the acoustic pulse is shown in gray.

pressure values, was chosen $T_0 = 17$ $\mu$s. Finally, for each distance, the averaged waveform was compared with the original ideal $N$-wave at the same distance. The correction to the duration of the compression phase of the averaged wave caused by the exposure time of the high-speed camera was found.

The reconstruction algorithm described above is valid under several assumptions. First, it is assumed that the method is valid despite the optical beam not being collimated as in classical schlieren systems.[27] However, this assumption is valid, since the width of the test zone, i.e., the zone where the light beam actually interacts with the refractive index inhomogeneities, is much smaller than the total beam length, which is equal to twice the radius of curvature of the mirror. Quantitatively, the width of the test zone is estimated as $2 \cdot \sqrt{2\lambda_{ac} r - \lambda_{ac}^2}$ [Fig. 2(b)] where $\lambda_{ac}$ is the wavelength of the acoustic wave. For a maximum propagation distance of 50 cm and a wavelength of 2 cm, the width of the test zone is 28 cm, which is small in comparison to 2 m of the beam length.

The second assumption is that the wave has a spherical wavefront in the $xy$ plane, thus the refractive index $n(r)$ is a function of only the radial distance $r$. In the experimental conditions, generally it is true; however, for large electrode gaps or small distances this assumption may be slightly violated.

The third assumption is that optical beam propagation is considered in the framework of geometrical optics [Eq. (4)]. Moreover, it is assumed that optical rays passing through the test zone remain straight lines [Eq. (2)]. These assumptions may be violated near strong shocks where diffraction effects are important.[12,31,32]

## III. RESULTS

In this section, reconstructed dimensionless waveforms are presented and analyzed at different distances from the spark source. To demonstrate how the exposure time of the high-speed camera affects the waveforms, results of numerical simulation are presented. The duration of the compression phase is analyzed as a function of propagation distance, which allows the absolute pressure values to be determined.

### A. Optical data treatment

A typical schlieren image of the spark-generated pulse measured in the $xz$ plane is shown in Fig. 3(a). Here the averaged background image was extracted to handle only the acoustical contribution to the inhomogeneities of the refractive index $n$. The radial symmetry of the wavefront was used to average the intensity signal and to greatly increase the signal to noise ratio. For this purpose the individual distributions of light intensity were calculated along 500 radial lines as shown in Fig. 3(a). A two dimensional (2D) interpolation was used for this calculation. Finally, these 1D distributions were averaged to obtain the resulting signal $I$ [Fig. 3(b)]. The inverse Abel transform is then applied to the signal [Eq. (8)] to calculate the waveform [Fig. 3(c)]. Details about

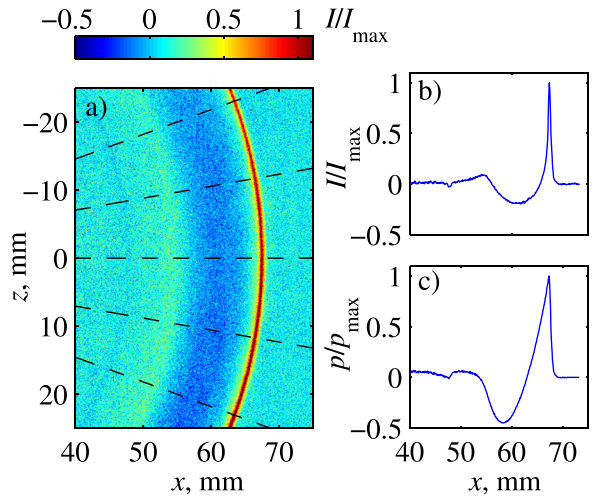


FIG. 3. (Color online) Illustration of the pressure signature reconstruction from the schlieren image. The light intensity with extracted background is shown in (a). Individual distributions of light intensity were calculated along 500 radial lines (examples are shown by dashed lines). The intensity signal averaged over 500 radial lines is shown in (b). Reconstructed waveform is presented in (c). All data shown in the figure are normalized by the corresponding maximum values.

numerical calculation of the integral in Eq. (8) are discussed in the Appendix.

Examples of waveforms, reconstructed at different distances from the spark source, are shown in Fig. 4. The analysis of optical data gives waveforms as functions of the distance from the source. Conversion of waveforms in time domain was done using the ambient sound speed $c_0$ which was equal to 343 m/s for the experimental conditions (relative humidity 49%, temperature 292 K).

The coordinate of the peak positive pressure is considered to be the propagation distance $r_0$ of the wave. Analyzing dimensionless waveforms plotted in Fig. 4, one can conclude that close to the source the acoustic wave is very asymmetric: the negative peak is significantly lower than the positive peak (waveform number 1 in Fig. 4) and the rear shock is very smooth and has a long rise time (about 15 $\mu$s in time which corresponds to 5 mm in space) in comparison to the front shock. These features are typical for the near field of blast waves.[18] The front shock is smeared to 3 $\mu$s due to the finite exposure time of the camera.

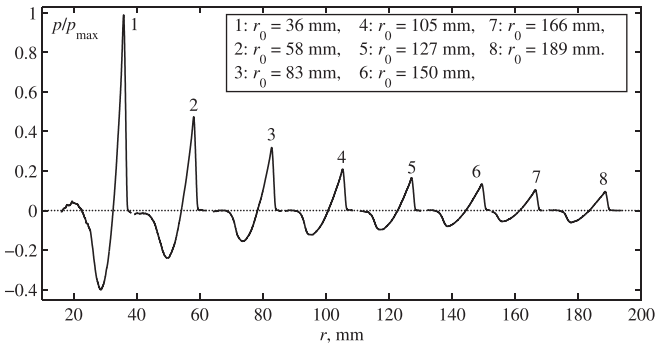


FIG. 4. Dimensionless waveforms reconstructed from the schlieren images at different distances from the spark source. For every pulse, the distance $r_0$ is defined as the coordinate of the peak positive pressure.

### B. Effect of the finite exposure time of the high-speed camera on the waveforms: Numerical simulation

Accurate estimation of the compression phase duration is a critical point of the method, since this parameter is used to determine the peak positive pressure. This subsection details how the compression phase duration of the real wave can be accurately determined from the measured waveform distorted by the averaging effect of the finite exposure time. The camera was assumed to perform a uniform temporal averaging of acoustic pressures arriving at this distance during the exposure time. To simulate this process, an $N$-wave was numerically propagated during the exposure time of 3 $\mu$s and then the averaging over all waveforms was performed for each distance.

A summary of the results of $N$-wave propagation modeling is presented in Fig. 5. The initial $N$-wave (solid curve) is supposed to imitate a "real" wave, while the averaged wave (dashed curve) is a "measured" wave. Note that in the space representation, the $N$-wave is no longer symmetric: there is a small difference between values of the peak positive and negative pressures. This is caused by the fact that the front shock is located farther from the source than the rear shock and thus has smaller amplitude because of the spherical divergence of the field. The distance between the propagated (dotted curve) and initial pulses corresponds to 3 $\mu$s and is about 1 mm.

The finite exposure time leads to the following effects. First, the coordinate of the peak positive pressure and the angles of smooth slopes (more than 3 $\mu$s in time or 1 mm in space) of the real and measured waveforms are unchanged. Second, the zero pressure position is shifted by a distance that corresponds to half of the exposure time (see markers at zero pressure level in Fig. 5). Finally, the whole duration of the measured wave becomes longer than the real one for a

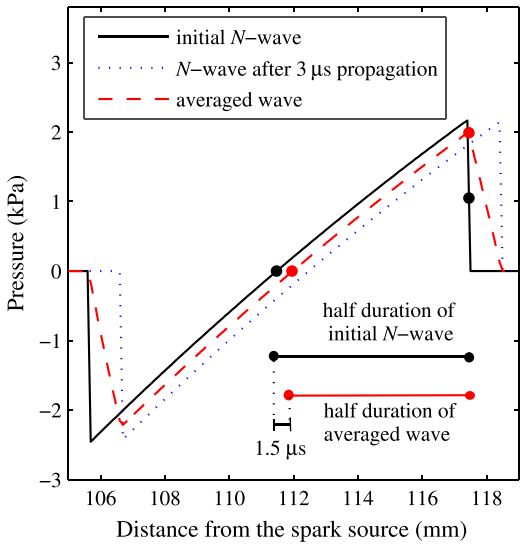


FIG. 5. (Color online) Effect of a 3 $\mu$s exposure time of the camera on the reconstructed waveform. Solid curve is the initial $N$-wave that was numerically propagated during 3 $\mu$s; dotted curve is the wave after propagation; dashed curve is the averaged wave, which imitates the measured waveform. The half duration of the initial wave can be calculated as the half duration of the averaged wave plus the half of the exposure time (1.5 $\mu$s).

time interval equal to the exposure time. Note also that the shock width (spatial equivalent of the rise time) obtained from the averaged waveform (1 mm) is determined by the exposure time (3 $\mu$s). To evaluate the duration of the compression phase correctly using the averaged wave, one should calculate the duration between the peak positive and zero pressure levels and add half of the exposure time, i.e., 1.5 $\mu$s in our case (lower right corner of Fig. 5). This method to properly evaluate the duration of the compression phase of the pulse is found to be applicable for all distances where the measurements were taken. Note, that nonlinear distortions of the propagated wave (dotted curve) are not significant and the correction to the half duration of the measured wave can be obtained based on the assumption of linear plane wave propagation.

### C. Estimation of the peak positive pressures from the pulse elongation

Using the results presented in the previous subsection, the duration of the compression phase was calculated as a function of the propagation distance for reconstructed dimensionless waveforms. To estimate the coefficient $\sigma_0$ in Eq. (9), experimental data for $(T/T_0)^2 - 1$ were linearly fitted as a function of $\ln(r/r_0)$ using the least squares method (Fig. 6). The origin of the graph in Fig. 6 corresponds to $T_0 = 13.5\ \mu$s and $r_0 = 70.5$ mm. Fifteen sparks were used to obtain the data presented in Fig. 6. The value of 0.486 was obtained for the coefficient $\sigma_0$ with a standard deviation of 0.013. The corresponding peak positive pressure was $p_0 = 2\gamma p_{\text{atm}} c_0 T \sigma_0/[(\gamma+1)r_0] = 3.72$ kPa. Finally, pressure amplitudes were found for all distances and thus pressure signatures were fully reconstructed. Note that the temporal correction of 1.5 $\mu$s to the duration of the compression phase was quite substantial—without taking into account the reconstructed pressure amplitudes would be up to 10% higher.

Reconstructed peak positive pressures at different distances from the spark source are shown in Fig. 7 (markers). The power law $p = p_0(r/r_0)^{-1.2}$ provides a good approximation of the peak pressure as a function of distance. Reed proposed in Ref. 33 this relation for blast waves and it is in good agreement with experimental values starting from about 100 mm from the source. The discrepancy between the Reed relation and experimental values closer to the spark source could be explained by less applicability of either the data processing method or the Reed relation. Nevertheless, both dependencies predict extremely high peak positive pressure close to the spark (about 12 kPa at the distance of 30 mm).

Examples of the reconstructed pressure signatures at different distances from the source are shown in Fig. 8. One can observe that close to the source the duration of the compression phase of the wave is about two times smaller than the duration of the rarefaction one (waveform at $r_0 = 36$ mm). As the acoustic wave propagates further from the source, it becomes more symmetric and the rear shock becomes steeper, the rise time reaches 3 $\mu$s, which is equal to the resolution time. The durations of compression and rarefaction phases of the wave equalize. Waveforms start to resemble an *N*-wave only starting from the distances of about $r_0 = 500$–$600$ mm, but even at the distance of $r_0 = 532$ mm (last subfigure) the wave is still not fully symmetric, the peak positive pressure being 1.2 times higher than the peak negative pressure. The measured front shock rise time is limited by the exposure time of the camera and equals to 3 $\mu$s which corresponds to a 1 mm shock thickness for all measured waveforms.

## IV. DISCUSSION

The optical schlieren method presented in this paper provides the attractive possibility to obtain quantitative information about characteristics of the high-amplitude and

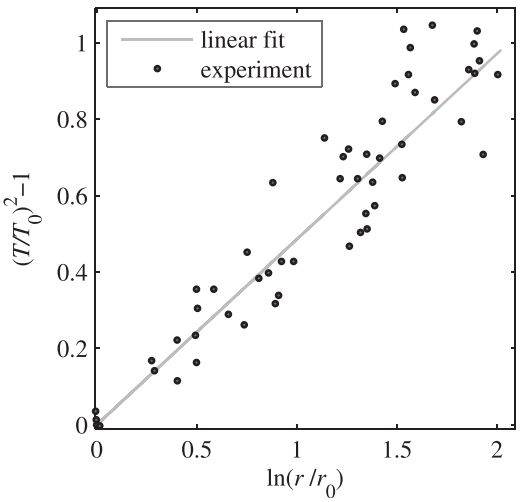


FIG. 6. Experimental (markers) data for the duration of the compression phase $T$ as a function of propagation distance $r$. The origin of the graph corresponds to $T_0 = 13.5\ \mu$s and $r_0 = 70.5$ mm. Solid line is obtained by linear fitting the experimental values using the method of least squares, the coefficient of proportionality equals 0.486 with standard deviation of 0.013.

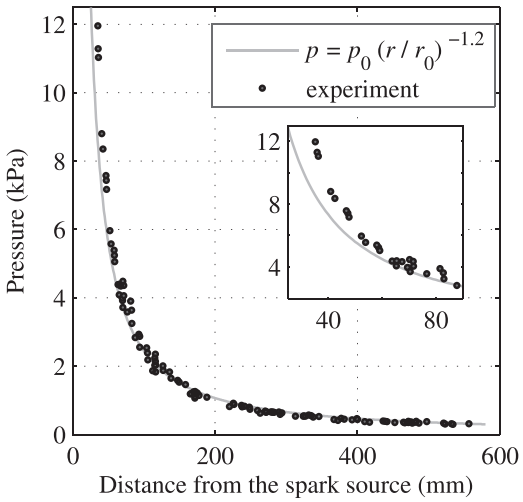


FIG. 7. Experimental (markers) values of the peak positive pressure at different radial distances from the spark source. Solid curve corresponds to the Reed formula $p = p_0(r/r_0)^{-1.2}$ dependence, where $p_0 = 3.72$ kPa at the distance $r_0 = 70.5$ mm. A zoom view of the data at small propagation distances is given in the inset.

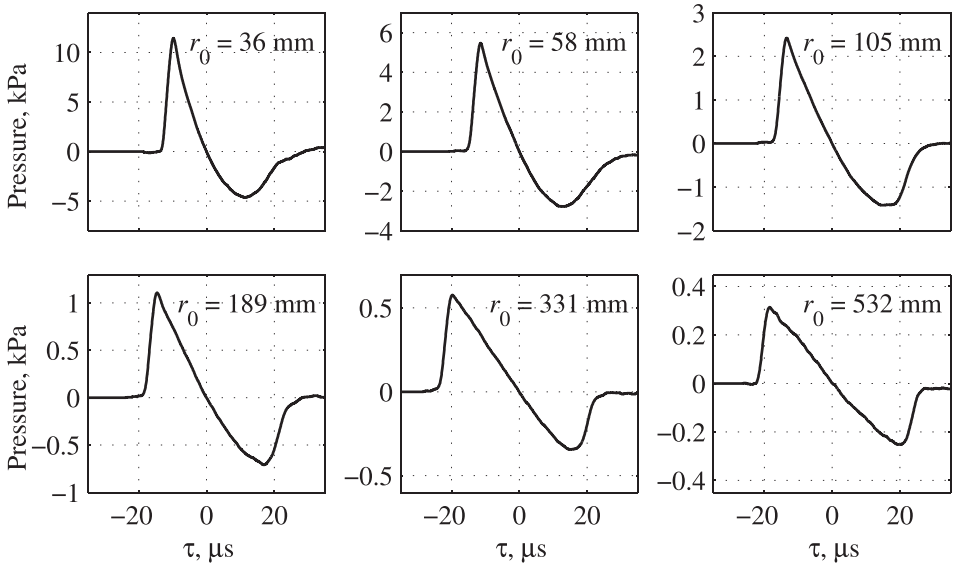


FIG. 8. Reconstructed temporal waveforms generated by the spark source. The radial position $r_0$ of the positive peak is noted in each subfigure.

short duration acoustic pulses generated by a spark in a homogeneous atmosphere. The time resolution of the method is mainly limited by the exposure time of the high-speed camera, which was 3 $\mu$s in our case. This resolution is not sufficient to describe the fine structure of shock fronts, but this method allows the rare fraction phase of the wave to be reconstructed. The optical schlieren method has advantages and disadvantages compared to two other techniques used in aeroacoustic measurements: microphone and optical focused shadowgraphy methods.

First, let us compare the schlieren method with measurements by condenser microphones. Microphone measurements usually start from 150 to 200 mm away from the source where the pressure levels are not very high and the response of the microphone is linear (maximum pressure level for a condenser microphone Bruel & Kjaer 1/8 in. type 4138 is approximately 2000 Pa or 160 dB re 20 $\mu$Pa). In contrast, there is no restriction on the minimal distance from the spark in the schlieren method: one can obtain a schlieren image even at 30 mm from the spark and the corresponding waveform could be reconstructed. Possibly, the data processing methodology is not highly accurate at distances very close to the spark, but nonetheless one can obtain an approximate waveform that could not be measured using microphones. Note also that in microphone measurements it is impossible to estimate distortions induced by the wave diffraction on the microphone, microphone mounting and its frequency response. Smearing of the schlieren image during the exposure time of the high-speed camera is the main cause of distortion. This distortion is quite predictable quantitatively (as discussed in Sec. III B).

The schlieren method has also some advantages with respect to the focused shadowgraphy technique described in Ref. 13. The contrast of shadowgrams (images obtained using the focused shadowgraphy technique) is proportional to the second spatial derivative of pressure, while the contrast of schlieren images is proportional to the gradient of pressure.[27] The focused shadowgraphy technique allowed visualizing the front shock of the pulse[12] with a time resolution better than 0.5 $\mu$s, which permitted to describe its fine structure. However, if this method is well suited to measure shocks, it is not sufficiently sensitive to measure the pressure decrease following the peak pressure nor the rear shock. The schlieren method is more sensitive to low amplitude pressure variations, and therefore makes it possible to estimate the whole waveform except the fine structure of the front shock (limitation due to the resolution of the camera). It should be possible to combine these two methods: first the front shock could be obtained using the focused shadowgraphy technique and it could then be replaced in a waveform obtained by the optical schlieren method.

The accuracy of the schlieren method is subject to ongoing investigations. Four main sources of error are identified. First, the distortion due to the exposure time of the camera; second, assumptions of geometrical optics and spherical symmetry in data processing; third, the low frequency noise associated with slow variations of background intensity between snapshots, which is substantial at large distances from the spark. Finally, although the spark source produces pulses with a good repeatability, their initial amplitude and duration changes from pulse to pulse. This leads to dispersion in experimental data (Fig. 6). With the current experimental setup, the uncertainty on the peak positive pressure estimation is on the order of 10%.

The measurement and the reconstruction methods reported here are important for the characterization of spark sources, especially at distances close to the spark, where direct acoustic measurements using acoustical condenser microphones are impossible because of the high pressure level. Although the experiments were performed in a homogeneous atmosphere, this method could be used also for the visualization and reconstruction of acoustical waveforms close to boundaries. This is the direction of our future studies.

## V. CONCLUSION

The propagation of nonlinear spark-generated acoustic pulses in homogenous air was studied experimentally using

the optical schlieren method. This method allowed reconstructing dimensionless waveforms at distances from 30 to 600 mm from the source. Analysis of schlieren images was based on the assumption of spherical geometry of the acoustic field and the geometrical optics approximations. The reconstruction of dimensionless acoustic waveforms was performed using the Abel-inversion transform. To evaluate the smearing of the waveform during exposure time of the camera, the propagation of a spherical diverging *N*-wave was simulated using the generalized Burgers equation. A method to evaluate the duration of the compression phase taking into account exposure time of the camera was proposed. The analysis of the elongation of the compression phase duration as a function of the propagation distance allowed to reconstruct the absolute pressure values. The time resolution of the method was restricted by the exposure time of the camera and thus the fine structure of the front shock could not be resolved using the method. The comparison between the optical schlieren method and two other known techniques for measurements of spark-generated shock waves was discussed. The present method has two main advantages. First, it allows reconstruction of the pressure signatures at distances close to the spark source (about 30 mm), where measurements using condenser microphones are impossible. Second, it provides the reconstruction of the whole waveform with the good accuracy that has not been achieved using the focused shadowgraphy method.[13]

## ACKNOWLEDGMENTS

This work has been partially supported by Russian Foundation for Basic Research (RFBR) grant 12-02-31830-mol_a, by the grant of the President of Russia No. MK-5895.2013.2, by the French National Research Agency (ANR) [research project "SIMMIC" (SIMI 9, ANR 2010 BLANC 0905 03), LabEx CeLyA ANR-10-LABX-60], and by the scholarship from the French Government. The authors are grateful to Jean-Michel Perrin for his help with the fabrication of the experimental setup, to Thomas Castelain and Benoît André for their help with the adjustment of the optical system, and to Olivier Marsden for the helpful comments on the manuscript.

## APPENDIX: NUMERICAL CALCULATION OF THE INVERSE ABEL TRANSFORM

Consider the numerical calculation of the integral $\int_r^{+\infty}(d/dx)(\int_x^{+\infty} I(r')dr')(dx/\sqrt{x^2-r^2})$ in Eq. (8), which is used to reconstruct the dimensionless waveform from the schlieren image. Inner integral $A(x)=\int_x^{+\infty} I(r')dr'$ is calculated using trapezoidal numerical integration while the outer integral contains a singularity at $x \to r$ and could not be calculated in this way. To avoid singularity, the integrand is approximated using a cubic spline interpolation and then calculated numerically.

Note that the investigated integral multiplied by the factor $(-1/\pi)$ is the Abel inversion transform that is written in general form as[29] $B(r)=-(1/\pi)\int_r^{+\infty}(dA/dx)(dx/\sqrt{x^2-r^2})$. One uses the next property of this inversion: $A=\int_x^{+\infty}(2rBdr/\sqrt{r^2-x^2})=-2\int_x^{+\infty}\sqrt{r^2-x^2}(dB/dr)dr$. Calculating the derivative, one finds $dA/dx=2\int_x^{+\infty}(dB/dr)(xdr/\sqrt{r^2-x^2})$. It follows that $(dA/dx)|_{x=0}=0$. Let us approximate $A(x)$ using cubic spline interpolation:

$$\begin{aligned} A(x) &= a_n + b_n(x-x_n) + c_n(x-x_n)^2 + d_n(x-x_n)^3 \\ &= \alpha_n + \beta_n x + \gamma_n x^2 + \delta_n x^3 \end{aligned} \tag{A1}$$

and assume that the function $A(x)$ is given at the nodes of the uniform grid $x_n=\Delta\cdot n,\ n=1,\ldots,N$, where $\Delta$ is the mesh spacing.

First, consider calculation for $r=0$: $B(r=0)=-(1/\pi)\int_0^{+\infty}(dA/dx)(dx/x)$. Split the integral for the sum of terms

$$B(r=0) = -\frac{1}{\pi}\int_0^{\Delta}\frac{dA}{dx}\frac{dx}{x} - \frac{1}{\pi}\sum_{n=1}^{n=N-1}\int_{n\cdot\Delta}^{(n+1)\cdot\Delta}\frac{dA}{dx}\frac{dx}{x}. \tag{A2}$$

Substituting the cubic spline approximation (A1) with $\beta_0=0$ [because $(dA/dx)|_{x=0}=0$] in Eq. (A2), one obtains

$$\begin{aligned} B(r=0) = &-\frac{1}{\pi}\left(2\gamma_0\Delta+\frac{3}{2}\delta_0\Delta^2\right) - \frac{1}{\pi}\sum_{n=1}^{n=N-1}\left[\beta_n\ln\left(\frac{b}{a}\right)\right. \\ &\left. + 2\gamma_n(b-a) + \frac{3}{2}\delta_n(b^2-a^2)\right], \\ &a=n\cdot\Delta,\quad b=(n+1)\cdot\Delta. \end{aligned} \tag{A3}$$

Second, consider calculation for $r=m\cdot\Delta,\ m=1,\ldots,N-1$. Let $A(x=N\cdot\Delta)=0$ because $A(x)\to 0$ if $x\to\infty$. Replace the integral by the sum of integrals over the segments: $B(r=m\cdot\Delta)=-(1/\pi)\sum_{n=m}^{n=N-1}\int_{n\cdot\Delta}^{(n+1)\cdot\Delta}(dA/dx)(dx/\sqrt{x^2-r^2})$. Using cubic spline approximation (A1) for every segment, one obtains

$$\begin{aligned} &B(r=m\cdot\Delta) = -\frac{1}{\pi}\sum_{n=1}^{n=N-1} I_n, \quad \text{where} \\ &I_n = \beta_n(b'-a') + 2\gamma_n c\left[sh(b')-sh(a')\right] \\ &\quad + \frac{3c^2\delta_n}{2}\left\{b'-a'+\frac{1}{2}\left[sh(2b')-sh(2a')\right]\right\}, \\ &\quad a'=arcch\left(\frac{a}{c}\right),\ b'=arcch\left(\frac{b}{c}\right),\ c=m\cdot\Delta. \end{aligned} \tag{A4}$$

Thus, using Eqs. (A3) and (A4) it is possible to calculate the Abel inversion transform numerically by summing the results for each segment. However, the light intensity $I$ is equal to zero for distances $x$ beyond the location of the pulse and therefore numerical integration requires a finite window. In numerical simulations, the size of spatial window was equal to the size of the schlieren image and the spatial step was 8 $\mu$m.

[1]B. Lipkens and D. T. Blackstock, "Model experiment to study sonic boom propagation through turbulence. Part I: Model experiment and general results," J. Acoust. Soc. Am. **103**, 148–158 (1998).

[2]B. Lipkens and D. T. Blackstock, "Model experiment to study sonic boom propagation through turbulence. Part II: Effect of turbulence intensity and propagation distance through turbulence," J. Acoust. Soc. Am. **104**, 1301–1309 (1998).
[3]B. Lipkens, "Model experiment to study sonic boom propagation through turbulence. Part III: Validation of sonic boom propagation models," J. Acoust. Soc. Am. **111**, 509–519 (2002).
[4]B. A. Davy and D. T. Blackstock, "Measurements of the refractive and diffraction of a short N wave by a gas-filled soap bubble," J. Acoust. Soc. Am. **49**, 732–737 (1971).
[5]P. Blanc-Benon, S. Ollivier, K. Attenborough, and Q. Qin, "Laboratory experiments to study *N*-waves propagation: Effects of turbulence and/or ground roughness," in *17th International Symposium on Nonlinear Acoustics*, Manchester, UK (2005), Vol. 838, pp. 651–654.
[6]M. Averiyanov, S. Ollivier, V. Khokhlova, and P. Blanc-Benon, "Random focusing of nonlinear acoustic *N*-waves in fully developed turbulence: Laboratory scale experiment," J. Acoust. Soc. Am. **130**(6), 3595–3607 (2011).
[7]E. Salze, P. Yuldashev, S. Ollivier, V. Khokhlova, and P. Blanc-Benon, "Laboratory-scale experiment to study nonlinear *N*-wave distortion by thermal turbulence," J. Acoust. Soc. Am. **136**, 556–566 (2014).
[8]V. Grillon, X. Meynial, and J. D. Polack, "What can auralisation in small scale models achieve?," Acta Acust. **82**, 362–364 (1996).
[9]J. Picaut and L. Simon, "A scale model experiment for the study of sound propagation in urban areas," Appl. Acoust. **62**, 327–340 (2001).
[10]M. Almgren, "Acoustic boundary layer influence on scale model simulation of sound propagation: Experimental verification," J. Sound Vib. **110**, 247–259 (1986).
[11]W. M. Wright, "Propagation in air of *N* waves produced by sparks," J. Acoust. Soc. Am. **73**, 1948–1955 (1983).
[12]P. Yuldashev, S. Ollivier, M. Averiyanov, O. Sapozhnikov, V. Khokhlova, and P. Blanc-Benon, "Nonlinear propagation of spark-generated *N*-waves in air: Modeling and measurements using acoustical and optical methods," J. Acoust. Soc. Am. **128**, 3321–3333 (2010).
[13]L. Orenstein, "The rise time of *N*-waves produced by sparks," Technical Report, Appl. Res. Lab., Univ. Texas Austin, ARL-TR-82-51 (1982).
[14]Q. Qin and K. Attenborough, "Characteristics and application of laser-generated acoustic shock waves in air," Appl. Acoust. **65**, 325–340 (2004).
[15]A. Loubeau, V. W. Sparrow, L. L. Pater, and W. M. Wright, "High-frequency measurements of blast wave propagation," J. Acoust. Soc. Am. **120**, EL29–EL35 (2006).
[16]J. W. M. DuMond, E. R. Cohen, W. K. H. Panofsky, and E. Deeds, "A determination of the waveforms and laws of propagation and dissipation of ballistic shock waves," J. Acoust. Soc. Am. **18**, 97–118 (1946).
[17]M. N. Plooster, "Shock waves from line sources. Numerical solutions and experimental measurements," Phys. Fluids **13**, 2665–2675 (1970).
[18]H. L. Brode, "Blast wave from a spherical charge," Phys. Fluids **2**, 217–229 (1959).
[19]P. V. Yuldashev, M. V. Averiyanov, V. A. Khokhlova, S. Ollivier, and P. Blanc-Benon, "Nonlinear spherically divergent shock waves propagating in a relaxing medium," Acoust. Phys. **54**, 32–41 (2008).
[20]M. Averiyanov, P. Blanc-Benon, R. O. Cleveland, and V. Khokhlova, "Nonlinear and diffraction effects in propagation of *N*-waves in randomly inhomogeneous moving media," J. Acoust. Soc. Am. **129**(4), 1760–1772 (2011).
[21]W. M. Wright and J. L. McKittrick, "Diffraction of spark-produced acoustic impulses," Am. J. Phys. **35**, 124–128 (1967).
[22]W. M. Wright and N. W. Medendorp, "Acoustic radiation from a finite line source with *N*-wave excitation," J. Acoust. Soc. Am. **43**, 966–971 (1968).
[23]T. Mizukaki, "Application of digital phase-shift holographic interferometry to weak shock waves propagating at Mach 1.007," Shock Waves **20**, 19–27 (2010).
[24]G. Smeets, "Laser interference microphone for ultrasonics and nonlinear acoustics," J. Acoust. Soc. Am. **61**, 872–875 (1977).
[25]B. André, T. Castelain, and C. Bailly, "Broadband shock-associated noise in screeching and non-screeching underexpanded supersonic jets," AIAA J. **51**(3), 665–673 (2013).
[26]B. André, T. Castelain, and C. Bailly, "Experimental exploration of underexpanded supersonic jets," Shock Waves **24**, 21–32 (2014).
[27]G. S. Settles, *Schlieren and Shadowgraph Techniques: Visualizing Phenomena in Transparent Media* (Springer-Verlag, Heidelberg, 2001), pp. 27, 39–52, 338–340.
[28]W. Merzkirch, *Flow Visualization* (Academic, New York, 1974), pp. 126–134.
[29]R. N. Bracewell, *The Fourier Transform and Its Applications* (McGraw-Hill, New York, 2000), pp. 351–353.
[30]A. D. Pierce, *Acoustics: An Introduction to Its Physical Principles and Applications* (Acoustical Society of America, New York, 1989), pp. 603–605.
[31]J. Panda and G. Adamovsky, "Laser light scattering by shock waves," Phys. Fluids **7**, 2271–2279 (1995).
[32]P. Yuldashev, M. Averiyanov, V. Khokhlova, O. Sapozhnikov, S. Ollivier, and P. Blanc-Benon, "Measurement of shock *N*-waves using optical methods," in *10eme Congres Francais d'Acoustique, Lyon*, CD (2010). Available online at https://tel.archives-ouvertes.fr/CFA2010-APU4/hal-00539747v1 (Last viewed 6 March 2015).
[33]J. W. Reed, "Atmospheric attenuation of explosion waves," J. Acoust. Soc. Am. **61**, 39–47 (1977).